

# Active Rectification For the Optimal Command of Bidirectional Resonant Wireless Power Transfer Robust to Severe Circuit Parameters Deviations

Alexis Desmoort , *Student Member, IEEE*, Olivier Deblecker , *Member, IEEE*, and Zacharie De Grève, *Member, IEEE*

**Abstract**—In this article, a method resorting to active rectification for the optimal control of a bidirectional resonant wireless power transfer system is proposed. Benefiting from a dual active bridge topology and without requiring any additional dc–dc converter, the real and the imaginary parts of the equivalent load impedance are modulated simultaneously and independently, for achieving optimal operating conditions despite circuit parameters deviations. Based on a first harmonic analysis, the methodology and its beneficial impacts against variations in the windings mutual inductance or against mistuned resonant capacitor are presented and illustrated. By an argued discussion, the proposed method extent is enlarged to changes in any circuit parameters. Time-domain simulations of the converters topology and command demonstrates the method effectiveness by achieving the system maximum efficiency. Controllability restrictions preventing the compensation of the most severe parameters variations are highlighted. Associated with the limited voltage producible by conventional full-bridge converters, the latter restrictions are surmounted with success by considering Z-source topologies for the front-end and back-end converters.

**Index Terms**—Active rectification, bidirectional power flow, dual active bridge, wireless power transmission (WPT), Z-source converter.

## I. INTRODUCTION

WIRELESS power transfer (WPT) is a popular and trending topic in the scientific and industrial communities. As a matter of fact, the recent progresses in power electronics have paved the way for the implementation of resonant inductive power transfer to energy-greedy applications, such as electric vehicle (EV) battery charging [1]–[3]. Bringing more convenience and more safety, wireless charging systems for EVs reach current performances comparable to or even better than classical wire-connected systems [4]. Dealing with high power-levels [from a

few kilowatt (kW) to tens of kW, typically] requires, however, to pay a particular attention on the system optimal operation, as each percent of its power efficiency represents a nonnegligible amount of power. Based on magnetically coupled resonant circuits, the WPT systems are only effective in a restricted operating range, with respect to the circuit parameters. An adequate command is, therefore, mandatory for practicable domestic and industrial implementations, which are subject to transmitter–receiver misalignment and/or components deteriorations.

The operating frequency is obviously a key parameter for optimizing the performances of a resonant system. Incidentally, the interest of an appropriate frequency variation has been demonstrated [5], [6]. However, variable-frequency control strategies are not addressed in this work as standardization procedures currently tend to impose a fixed frequency for improving WPT systems universality. Moreover, the typical bifurcation phenomenon occurring with resonant coupling threatens the stability and the controllability of the system when the variation in frequency is too important [7]. With a fixed operating frequency, optimal performances can be reached by a suitable sizing of the system load resistance [8]. Based on the latter statement, fixed-frequency control strategies have successfully investigated the modulation of the apparent resistive load, thanks to a dc–dc converter interfacing the circuit and the load [9], [10]. Colak *et al.* [11] have further demonstrated the possibility to avoid any additional dc–dc converter while modulating the apparent load by using a semibridgeless active rectifier instead of a conventional diode rectifier for interfacing the secondary circuit with the actual load. Although effective, those strategies aim to solely optimize the active power flow, whereas the reactive power flow—preponderant for a proper resonant operation—is free to vary with the potential deviations in circuit parameters. Therefore, research works have recently investigated the resort to a full-bridge active rectifier for introducing a given phase shift between the primary and the secondary voltages. Zhao *et al.* [12] have, e.g., illustrated the feasibility of using the nonsynchronous rectification for influencing the reactive power flow and further the resonance phenomenon, with nevertheless a simultaneous impact on the optimality of the active power flow. Based on the latter work, an advanced contribution proposed to modulate independently the resistive and the reactive parts of the equivalent load via active rectification for maximizing

Manuscript received July 2, 2019; accepted September 13, 2019. Date of publication January 12, 2020; date of current version March 17, 2020. Paper no. 2019-IPCC-0622, presented at the 2018 International Symposium on Power Electronics, Electrical Drives, Automation and Motion, Amalfi, Italy, Jun. 20–22, and approved for publication in the IEEE TRANSACTIONS ON INDUSTRY APPLICATIONS by the Industrial Power Converter Committee of the IEEE Industry Applications Society. (*Corresponding author: Alexis Desmoort.*)

The authors are with the Electrical Power Engineering Unit University of Mons, 7000 Mons, Belgium (e-mail: alexis.desmoort@umons.ac.be; olivier.deblecker@umons.ac.be; zacharie.degrevé@umons.ac.be).

Color versions of one or more of the figures in this article are available online at <https://ieeexplore.ieee.org>.

Digital Object Identifier 10.1109/TIA.2020.2966161

the efficiency and increasing the deliverable power [13]. To this end, the optimal conditions are obtained numerically via a constrained optimization, and an active rectifier followed by an additional dc–dc converter is employed for achieving those conditions, by respectively and independently controlling the secondary voltage phase shift and regulating its amplitude.

In this article, we propose an alternative approach to optimize WPT performances via active load modulation with two main simplification axes. On the one hand, a nonsynchronous rectification is performed by controlling an active rectifier using a symmetric voltage cancellation (SVC) command, enabling the combined control of the amplitude and of the phase of the secondary voltage without any additional dc–dc converter. It results in a topological symmetry, which provides power-reversibility capabilities for the resonant WPT system, which is a farsighted asset since enabling bidirectional powerflows permits to use EVs as storage units for vehicle-to-home and vehicle-to-grid applications [14]. In contrast, the aforementioned state-of-the-art contributions use asymmetric topologies and are only practicable for a unidirectional power flow. Furthermore, the optimal conditions are here obtained analytically via a simple first harmonic analysis (FHA) of the system equivalent circuit. Both the real and the imaginary parts of the equivalent load impedance are in that way independently controlled for keeping optimal performances and supplying a fixed power despite deviations. Preliminarily presented in [15], this method is subject to restrictions in controllability associated with the limited voltage attainable by conventional converters. For overcoming those restrictions, Z-source converters [16] are investigated in this article. In the context of WPT, Z-source converters have already been envisioned as front-end converters for improving the systems operation, notably via a power factor correction [17]–[19]. Here, Z-source converters are employed both as an inverter on the source side and as an active rectifier on the load side. To our knowledge, using a Z-source active rectifier has not been proposed yet in the framework of WPT.

The article is organized as follows. In Section II, the FHA of the proposed WPT topology is proceeded. In Section III, the methodology to achieve these optimal conditions via synchronous rectification is detailed. The proposed approach is validated and analyzed by observing the results obtained under FHA assumptions. Section IV is dedicated to the implementation of the power converters in the time domain, highlighting restrictions in the controllability, which are in turn discussed. For surmounting the latter restrictions, the Z-source concept is outlined. Section V exposes the theoretical bases for Z-source converters and presents the results given by the time-domain implementation of the Z-source converters command following the proposed approach.

## II. FHA OF THE PROPOSED TOPOLOGY

The proposed resonant WPT system topology is presented in Fig. 1. The power transfer is ensured by a near-field magnetic coupling between the primary and secondary windings, with a mutual inductance  $M$ . For reducing the volt–ampere (VA) rating of both ac circuits, the reactive power flow is cancelled

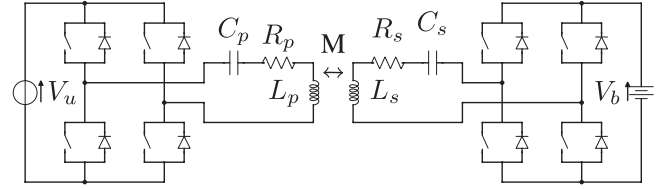


Fig. 1. Proposed resonant WPT topology.

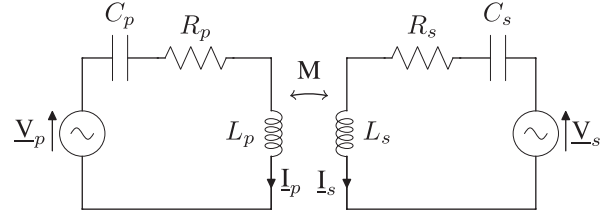


Fig. 2. Equivalent circuit for FHA.

by compensating the series self-inductance of each side  $L_p$  and  $L_s$  by a series capacitance  $C_p$  and  $C_s$ , respectively. The system is designed so that the primary and the secondary circuits share a common self-resonant frequency  $\omega_0$ , calculated as

$$\omega_0 = \frac{1}{\sqrt{L_p C_p}} = \frac{1}{\sqrt{L_s C_s}}. \quad (1)$$

Operated with an angular frequency  $\omega$  equal to  $\omega_0$ , the system displays a theoretical infinite power transfer capability whereas presenting a unitary power efficiency. In practice, these transfer performances are limited by the components parasitic resistances  $R_p$  and  $R_s$ . Each circuit is connected to a full-bridge converter interfacing the resonant WPT system with the rectified utility voltage  $V_u$  on one side and with the battery voltage  $V_b$  on the other side. Considering the filtering action of each LC circuit on the converters ac currents, an FHA performed on the equivalent circuit shown in Fig. 2 is sufficient to analyze the system performances and operation. The power converter can be replaced by ac voltage sources as their ac voltage is controllable in module and phase via SVC. For clarity purposes, only the case of a power transfer from the utility to the battery is addressed in the following developments. Given the system topological symmetry, the case of a transfer from the battery to the utility can be treated similarly by interchanging the primary and the secondary roles in the mathematical expressions.

### A. Power Efficiency and Optimal Load

For analyzing the power efficiency and given the direction of the useful power, the source  $V_s$  is replaced by an equivalent active load  $Z_L = R_L + jX_L$ . Hence, the active power efficiency can be written as

$$\eta = \frac{R_L I_s^2}{R_p I_p^2 + R_s I_s^2 + R_L I_s^2} \quad (2)$$

where  $I_p$  and  $I_s$  are the rms values of the primary and the secondary currents, respectively. The combined primary and secondary circuits resonances are mandatory for maximizing

the power efficiency as the cancellation of the reactive power flow ensures a minimal value for  $I_p$  and  $I_s$ . In this resonant state, the primary and secondary currents can be related as

$$\omega_0 M I_p = (R_s + R_L) I_s. \quad (3)$$

Therefore, the power efficiency  $\eta$  becomes

$$\eta = \frac{R_L}{R_p \frac{(R_s + R_L)^2}{\omega_0^2 M^2} + R_s + R_L} \quad (4)$$

which depends on the windings intrinsic parameters such as  $R_p$ ,  $R_s$ , or  $M$  and on  $R_L$ , which can be modulated by controlling adequately the secondary power converter. Hence, the transfer efficiency can be optimized by imposing an optimal load  $R_L^{\text{opt}}$  so that

$$\frac{\partial \eta}{\partial R_L} (R_L^{\text{opt}}) = 0 \text{ and } \frac{\partial^2 \eta}{\partial R_L^2} (R_L^{\text{opt}}) < 0. \quad (5)$$

After solving (5), the optimal load is given by

$$R_L^{\text{opt}} = R_s \sqrt{1 + \frac{\omega_0^2 M^2}{R_p R_s}}. \quad (6)$$

Ensuring  $R_L = R_L^{\text{opt}}$  guarantees to operate the system at its maximum intrinsically achievable efficiency  $\eta_{\text{max}}$ , which is imposed by the design of the  $LC$  circuits and given by

$$\eta_{\text{max}} = \frac{\omega_0^2 M^2}{R_p R_s \left(1 + \sqrt{1 + \frac{\omega_0^2 M^2}{R_p R_s}}\right)^2}. \quad (7)$$

### B. Direct Modulation of the Load Impedance

The combination of an active rectifier with well-designed resonant WPT circuits offers a direct control on the load impedance. By applying the Kirchhoff's voltage law in FHA to the circuit presented in Fig. 2, one has

$$\underline{V}_p = \underline{Z}_p \underline{I}_p + j\omega M \underline{I}_s \quad (8)$$

$$\underline{V}_s = \underline{Z}_s \underline{I}_s + j\omega M \underline{I}_p \quad (9)$$

with  $j$  the imaginary unit (so that  $j = \sqrt{-1}$ ) and with

$$\underline{Z}_p = R_p + j\omega L_p + 1/j\omega C_p \quad (10)$$

$$\underline{Z}_s = R_s + j\omega L_s + 1/j\omega C_s. \quad (11)$$

Solving (8) and (9), the expressions of the currents are

$$\underline{I}_p = \frac{\underline{Z}_s \underline{V}_p - j\omega M \underline{V}_s}{\underline{Z}_p \underline{Z}_s + \omega^2 M^2} \quad (12)$$

$$\underline{I}_s = \frac{\underline{Z}_p \underline{V}_s - j\omega M \underline{V}_p}{\underline{Z}_p \underline{Z}_s + \omega^2 M^2}. \quad (13)$$

By observing (13), one can observe that the secondary current  $\underline{I}_s$  is quasi-independent from the secondary voltage  $\underline{V}_s$  at the resonant frequency  $\omega_0$ , as  $\underline{Z}_p = R_p \approx 0$  at  $\omega_0$  for properly designed coils. Therefore, modifying  $\underline{V}_s$  amounts to modulate directly the equivalent load impedance  $\underline{Z}_L$  as seen from the

secondary terminals is defined as

$$\underline{Z}_L = -\underline{V}_s / \underline{I}_s. \quad (14)$$

As a consequence, the real and imaginary parts of the equivalent load impedance can be adjusted independently by controlling the secondary voltage  $\underline{V}_s$  in module and in phase. On the other hand, the transferred power can be regulated by controlling the primary voltage  $\underline{V}_p$ , which determines  $\underline{I}_s$ .

## III. METHODOLOGY

Assuming that the system is operated at the primary self-resonant frequency (i.e.,  $\omega = 1/\sqrt{L_p C_p}$ ), the direct modulation of the load impedance is practicable, as described above. The control strategy consists in simultaneously maximizing the power efficiency and setting the output power.

### A. Maximization of the Power Efficiency

According to the developments mentioned above, the system achieves its maximum intrinsic power efficiency  $\eta_{\text{max}}$  when the secondary total reactance is null while the equivalent load resistance seen from its terminals is  $R_L^{\text{opt}}$ . The equivalent load impedance  $\underline{Z}_L$  must be equal to

$$\underline{Z}_L = R_L^{\text{opt}} + jX_L^{\text{opt}} \quad (15)$$

where  $X_L^{\text{opt}}$  ensures the cancellation of the reactive power in the secondary circuit in the case of a mistuned secondary circuit (i.e., when  $L_p C_p \neq L_s C_s$ ), with

$$X_L^{\text{opt}} = \frac{1}{\omega C_s} - \omega L_s. \quad (16)$$

One can note that  $X_L^{\text{opt}}$  is null when the secondary is correctly tuned (i.e., when  $\omega = 1/\sqrt{L_p C_p} = 1/\sqrt{L_s C_s}$ ). The secondary voltage can be shifted in phase for emulating a reactive function, thanks to the active rectification, which is not practicable with classical topologies. Mathematically, the condition for achieving  $\eta_{\text{max}}$  is written as

$$\underline{V}_s = -\underline{Z}_L^{\text{opt}} \underline{I}_s. \quad (17)$$

By eliminating the current (13) in (17), the condition becomes

$$j\omega \underline{Z}_L^{\text{opt}} M \underline{V}_p + \left( \underline{Z}_p \underline{Z}_s + \omega^2 M^2 + \underline{Z}_L^{\text{opt}} \underline{Z}_p \right) = 0 \quad (18)$$

which is a first equation linking the complex values  $\underline{V}_p$  and  $\underline{V}_s$ . One can observe that the condition (18) accounts for the parasitic resistances in the relation between  $\underline{V}_s$  and  $\underline{I}_s$ .

### B. Setting the Output Power

Achieving a reference active power  $P_{\text{ref}}$  to the load is accomplished by setting adequately the module of the secondary current. Indeed, assuming that condition (18) is achieved, the real part of the load is equal to  $R_L^{\text{opt}}$  so that a power  $P_{\text{ref}}$  is transmitted to the load when

$$I_s = \sqrt{P_{\text{ref}} / R_L^{\text{opt}}}. \quad (19)$$

Considering (13) and reminding that  $\underline{Z}_p \approx 0$ , the current  $\underline{I}_s$  lags the voltage  $\underline{V}_p$  (taken as the phase reference) by  $\pi/2$  radians, so

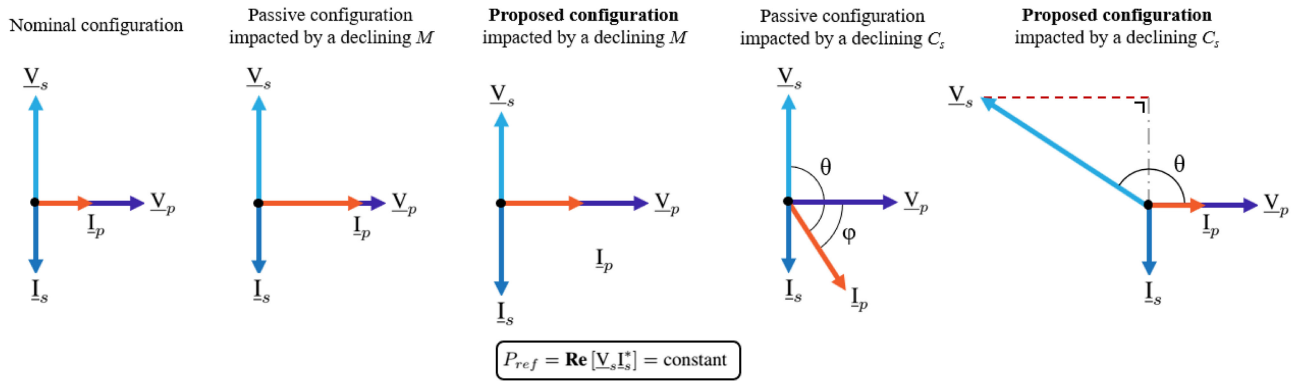

 Fig. 3. Voltages and currents phasors relative to a decrease of  $M$  and to a decrease of  $C_s$ .

 TABLE I  
 NOMINAL PARAMETERS OF THE TEST-CASE CIRCUIT

$f$	$R_p = R_s$	$L_p = L_s$	$C_p = C_s$	$M$
85 kHz	0.1 $\Omega$	70 $\mu\text{H}$	50 nF	8 $\mu\text{H}$

that the complex condition ensuring the transfer of a power  $P_{\text{ref}}$  is

$$\underline{I}_s = \sqrt{P_{\text{ref}}/R_L^{\text{opt}}} e^{-j\frac{\pi}{2}}. \quad (20)$$

From (13) and (20), the condition becomes

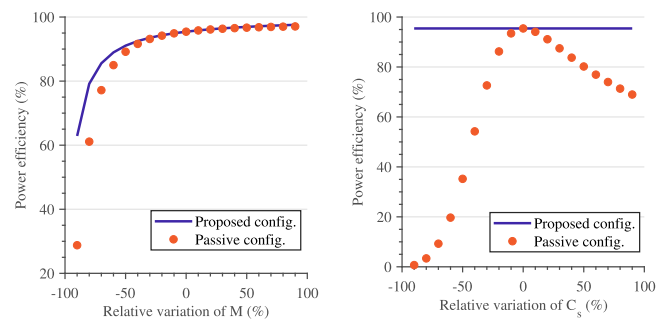
$$\frac{Z_p \underline{V}_s - j\omega M \underline{V}_p}{Z_p Z_s + \omega^2 M^2} = \sqrt{P_{\text{ref}}/R_L^{\text{opt}}} e^{-j\frac{\pi}{2}} \quad (21)$$

which is a second equation linking the values  $\underline{V}_p$  and  $\underline{V}_s$ . Finally, the desired setting point is reached by imposing the voltages  $\underline{V}_p$  and  $\underline{V}_s$  solving simultaneously (18) and (21).

### C. Illustration

The main principle of the methodology is illustrated on a test-case via MATLAB simulations. The nominal circuit parameters are gathered in Table I (with  $f = \omega/2\pi$  the operating frequency). The system is expected to supply a reference output power  $P_{\text{ref}} = 3.7$  kW to the load. For comparison purposes, the optimal performances of the proposed system are contrasted with the performances of a *passive* system, which is optimally designed for the nominal value of the circuit parameters only. Two illustration examples are considered. First, the decrease of the mutual inductance  $M$  is addressed as the most important case because very likely and frequently occurring during the system operation (due to windings misalignment). Impacting  $R_L^{\text{opt}}$ , such a case challenges the active power modulation of the proposed method. Second, the decrease of  $C_s$  (e.g., due to the deterioration of the related capacitor) is tackled. Rarely happening during the system operation but impacting  $X_L^{\text{opt}}$ , this case permits to validate the reactive power modulation abilities of the proposed system.

Observing the voltages and currents phasors (see Fig. 3) permits an intuitive understanding of the action of the proposed


 Fig. 4. Evolution of the different configurations power efficiency for variations of  $M$  (left) and of  $C_s$  (right).

method. For a passive configuration, a decline in  $M$  increases significantly the primary current  $\underline{I}_p$ , since the system has to achieve a constant output power despite harsher coupling conditions. The power efficiency is deteriorated due to increased Joule losses (see the left graph in Fig. 4). Facing up those conditions, the proposed method takes an action on the voltages  $\underline{V}_p$  and  $\underline{V}_s$  for a fairer repartition of the losses in the circuit, by increasing and decreasing the currents  $\underline{I}_s$  and  $\underline{I}_p$ , respectively. Despite an  $M$  decrease, the proposed configuration achieves, hence, the maximum efficiency. The latter is, therefore, optimal but inevitably lower than the nominal efficiency due to the detrimental effect of a diminution of  $M$  on the maximum intrinsically achievable efficiency [as described by (7)]. Also, the VA ratings are smaller on both sides. For passive configurations, a lowering of  $C_s$  raises drastically the primary current  $\underline{I}_p$ , since the system has to achieve a constant output power despite an increasing phase shift  $\varphi$  between the primary current  $\underline{I}_p$  and voltage  $\underline{V}_p$ . As a consequence, the system efficiency drops significantly due to Joule losses (see the right graph in Fig. 4). By performing an active rectification, the proposed method shifts the secondary voltage  $\underline{V}_s$ , which sweeps the solidary current  $\underline{I}_p$  away (as  $\theta$  is constant for a given variation of  $C_s$ ) until its alignment with the voltage  $\underline{V}_p$ . The mistuning penalty is displaced from the primary current  $\underline{I}_p$  to the secondary voltage  $\underline{V}_s$ , with a consequential rise of the secondary VA rating. However, both currents  $\underline{I}_p$  and  $\underline{I}_s$  are back in their nominal position so that the

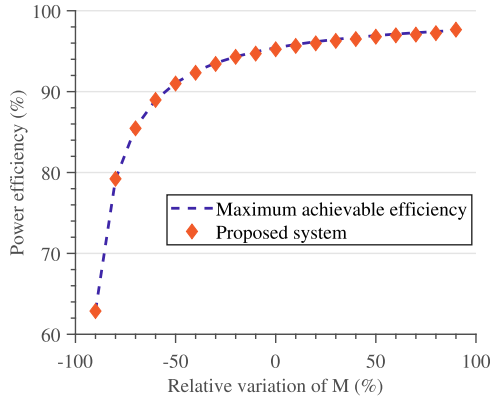


Fig. 5. Simulated measurement of the power efficiency for a deviation of  $M$  impacting the proposed system.

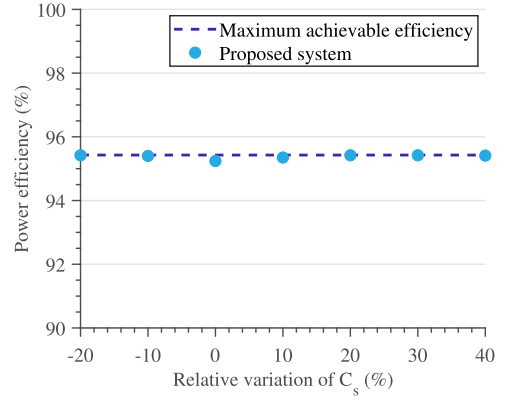


Fig. 6. Simulated measurement of the power efficiency for a deviation of  $C_s$  impacting the proposed system.

deleterious impact of a  $C_s$  variation on the system efficiency is fully compensated. One can notice that a spontaneous rise of  $C_s$  is unlikely in practice. However, illustrating such a case in Fig. 4 permits to virtually demonstrate the intrinsic compensation capabilities of the system. As a matter of fact, these two examples can be extended to deviations of any other circuit parameter. Holistically, variations of  $R_p$  and  $R_s$  have similar effects as  $M$  variations and can, thus, be compensated analogously. The same philosophy prevails between  $L_s$  variations and  $C_s$  variations. Finally, variations of  $L_p$  and/or  $C_p$  produce a deviation of the working angular frequency  $\omega$ , which can be compensated as combined deviations of  $M$  and  $C_s$ .

IV. VOLTAGE-SOURCE CONVERTERS IMPLEMENTATION

So far, the methodology has been developed and illustrated considering ideal and sinusoidal voltage sources. In this section, the actual voltage-source converters (see Fig. 1) and the related pulsewidth modulation commands are practically implemented in a realistic time-domain model running under the PSIM software. Consistently, the WPT test case described in Table I is anew considered. The time-step is fixed to  $10^{-7}$  s. MOSFETS have been selected as actual switching devices, and the voltages  $V_u$  and  $V_b$  are both fixed to 400 V in compliance with utility and EV batteries common voltage levels. The converters are controlled following an SVC scheme and produce voltages presenting fundamentals, which satisfy (18) and (21).

A. Time-Domain Simulation Results

Mutual inductance  $M$  and secondary capacitance  $C_s$  variations are applied to the system. This time-domain implementation aims to verify the relevance of the FHA-based methodology, despite the enriched harmonic content of the actual voltage waves. The corresponding time-domain results are compared to target operating points computed in the frequency domain (see Figs. 5–7). One can ascertain that the proposed methodology leads to an optimal operation of the system, despite parameters deviations. Notably, the aforementioned  $LC$ -circuits filtering effect is demonstrated by the proximity of time-domain and

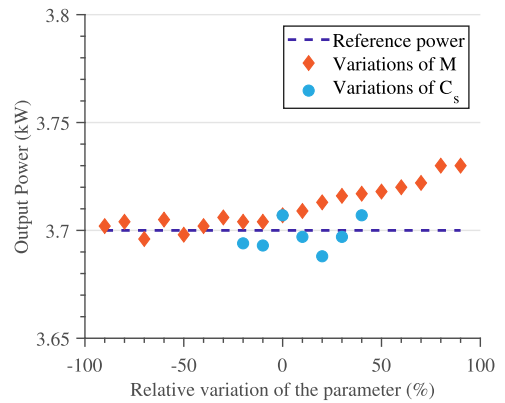


Fig. 7. Simulated measurement of the output power for deviations of  $M$  and  $C_s$  impacting the proposed system.

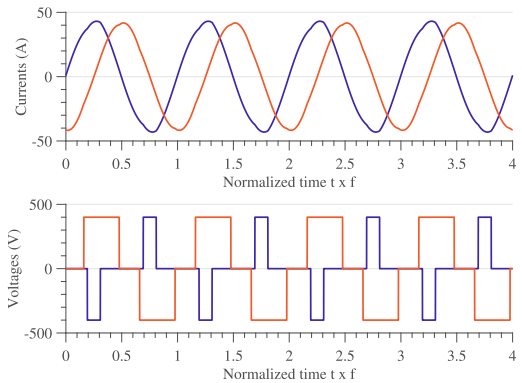


Fig. 8. Simulated primary (blue) and secondary (orange) waveforms from the proposed system for a  $-20\%$   $C_s$  deviation.

frequency-domain results and is qualitatively appreciable by observing currents waveforms shown in Fig. 8. The latter findings legitimate the FHA-based methodology despite nonsinusoidal voltage waveforms. The system performs with a clear effectiveness when facing the key-case of a coupling variation. However, the applicability of the proposed approach is restricted since the simulated system is not able to compensate  $C_s$  variations greater

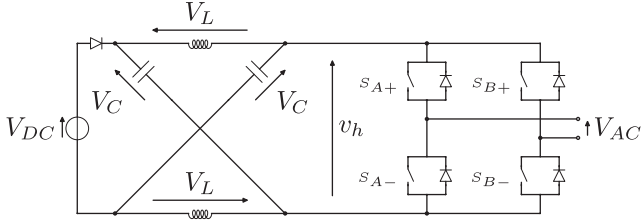


Fig. 9. Z-source converter.

than  $-20\%$  or  $+40\%$ . This restriction correlates with the limited voltage range of the converters, as discussed hereafter.

### B. Highlight on the Controllability Restrictions

Among the different nonidealities of conventional voltage-source converters, the limitation in producible voltage is the cause of the aforementioned controllability restrictions. As a matter of fact, the amplitude of the voltage on the converter ac-side is limited by the dc-side voltage source. Implementing an SVC command, the rms value  $V_{AC}^{(1)}$  of the fundamental of the ac voltage produced by a converter is

$$V_{AC}^{(1)} = \frac{2\sqrt{2}}{\pi} V_{DC} \sin(\beta/2) \quad (22)$$

where  $V_{DC}$  is the voltage on the dc-side of the converter (which is *a priori* fixed by the related source) and  $\beta$  is the SVC conduction angle. As a consequence, the maximal practicable ac voltage module is  $\frac{2\sqrt{2}}{\pi} V_{DC}$ , so that some solutions of (18) and (21)—requiring primary and/or secondary rms voltage higher than  $\frac{2\sqrt{2}}{\pi} V_u$  and  $\frac{2\sqrt{2}}{\pi} V_b$ , respectively,—are not achievable in practice. Yet, in the aforementioned case of a variation of  $C_s$ , the proposed method tends to largely increase the module of the secondary voltage for shifting it while keeping constant the output power, as shown in Fig. 3 and as previously explained. Compensations for severe  $C_s$  deviations are henceforth not reachable with the secondary converter, since the latter is not able to achieve a sufficient voltage. Although not addressed with the featured simulations, other situations can lead to similar issues and can also be pertaining to the primary converter (e.g., in the case of the setting of a higher reference power  $P_{ref}$ ). Reversible boost converters could be a solution to this issue complying with the power bidirectionality requirements. Nevertheless, this choice would lead to the inclusion of additional converters, which is a practice that we criticized in our state-of-the-art analysis. Hence, a transition to Z-source topologies is an elegant and a consistent way to extend the method applicability without requiring extra power converters.

## V. EXTENSION OF THE METHOD APPLICABILITY USING THE Z-SOURCE TOPOLOGY

A Z-source converter [16] is a unique structure combining a specific impedance network with a conventional converter adequately commanded (see Fig. 9). Developed for notably overcoming the drawbacks of voltage-source converters, the Z-source topology enables the generation of ac voltages with any

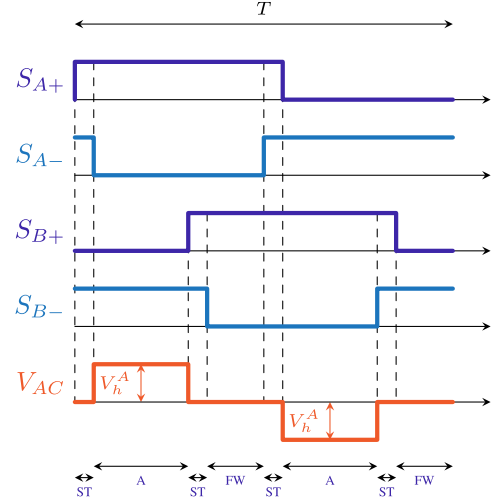


Fig. 10. Proposed Z-source converters control scheme.

value between zero and infinity theoretically. The development leading to this particular feature is detailed hereafter.

### A. Impedance Network and Shoot-Through State

The Z-source impedance network consists in a two-port network including two inductors interconnected with two cross-shaped capacitors. Presenting current limitation properties, this specific topology tolerates the shorting of the converter legs (i.e., the closing of both switching devices equipping a same leg), which is forbidden with a conventional converter for ensuring its integrity. In addition to the conventional active (i.e., when the converter produces a nonzero voltage) and freewheeling (FW) states, the Z-source converter disposes of an extra state corresponding to the shorting of one of its legs, called the *shoot-through* (ST) state. An additional diode protects the dc voltage source from hazardous current during ST states. Combined with the reactive nature of the Z-source impedance network, the ST state grants an additional degree of freedom in the converter command for achieving any output voltage.

### B. Circuit Analysis

For simplicity purposes, we assume that both inductors and both capacitors have, respectively, the same inductance and the same capacitance, making the Z-source network symmetric. Moreover, the common inductance and capacitance are supposed to be high enough for considering the inductors equal currents  $I_L$  and the capacitors equal voltages  $V_C$  constant. Focusing on the elementary analysis of the Z-source converter operation, the active (A) and FW states can be treated similarly. During these states (prevailing, respectively, for total portions  $D_A$  and  $D_{FW}$  of the period  $T$ ), the voltages in the circuit are

$$v_L = V_{DC} - V_C \quad v_h = 2V_C - V_{DC}. \quad (23)$$

During the ST state (prevailing for a total portion  $D_{ST}$  of the period  $T$ ), the voltages in the circuit are

$$v_L = V_C \quad v_h = 0. \quad (24)$$

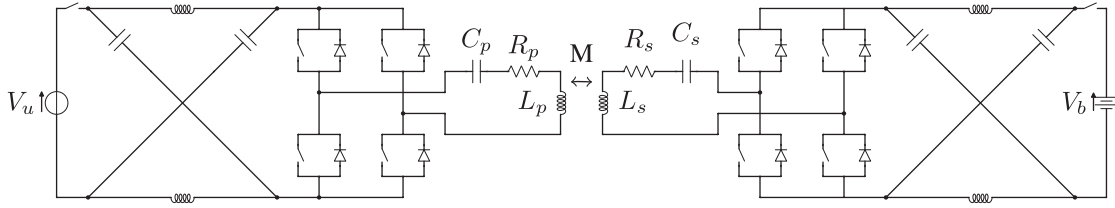


Fig. 11. Improved proposition of resonant WPT topology.

In the steady state, the system is characterized by the absence of net energy storage in the reactive elements on a working period. Notably, the mean inductors voltage  $\bar{v}_L$  must be null. One has

$$\bar{v}_L = (D_A + D_{FW})(V_{DC} - V_C) + D_{ST}V_C = 0 \quad (25)$$

leading to the value of the capacitors voltage  $V_C$  calculated as

$$V_C = \frac{1 - D_{ST}}{1 - 2D_{ST}} V_{DC}. \quad (26)$$

When the converter is in the active state, the voltage on the dc-side of the full-bridge  $V_h^A$  is theoretically constant and equal to

$$V_h^A = 2V_C - V_{DC} = \frac{1}{1 - 2D_{ST}} V_{DC}. \quad (27)$$

During the active states, the Z-source converter can, therefore, produce a dc voltage  $V_h^A$  ranging from  $V_{DC}$  to infinity by introducing ST states with  $0 \leq D_{ST} < 0.5$ . As a consequence, the module of the fundamental ac voltage produced by the converter can be worth any value between zero and infinity. Here, a variant of an SVC command integrating ST states while ensuring a uniform repartition of the constraint on the switches (in terms of conduction time and STs) is proposed. Referring to the notations shown in Fig. 9, the corresponding gate signals of the switches and the resulting ac voltage are represented in Fig. 10. Under those conditions, the rms value of the fundamental of the Z-source converter ac voltage is given by

$$V_{AC}^{(1)} = \frac{2\sqrt{2}}{\pi} \frac{V_{DC}}{1 - 2D_{ST}} \sin \left[ \frac{(1 - D_{ST} - D_{FW})\pi}{2} \right] \quad (28)$$

which can take any value between zero and infinity by an adequate choice of  $D_{ST}$  and  $D_{FW}$ . Therefore, the restrictions experienced in Section IV are overcome without any additional converter. Finally, one can notice that the present development does not rely on the current direction so that the Z-source topology complies with our reversibility requirements by replacing the dc-source diode by a bidirectional switch.

### C. Implementation and Discussions

Z-source impedance networks are introduced on both primary-side and secondary-side converters (see Fig. 11 for the resulting circuit). The problematical case of a  $C_s$  variation is anew considered with this improved circuit. The time-domain simulation of the latter is carried out on the PSIM software, and the associated results are presented in Figs. 12 and 13. One can observe the positive impact of the Z-source converters on the

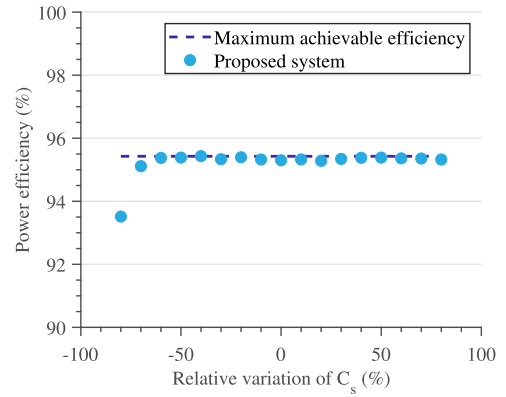


Fig. 12. Simulated measurement of the power efficiency for a deviation of  $C_s$  impacting the improved system.

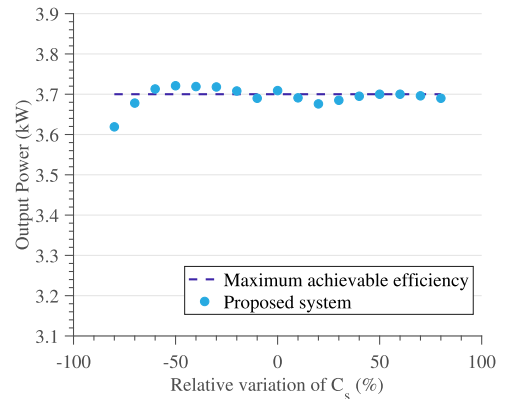


Fig. 13. Simulated measurement of the output power for a deviation of  $C_s$  impacting the improved system.

extent of the proposed method. Nonetheless, the two most severe decreases in  $C_s$  deviate slightly from the expected set points. Actually, the required fundamental rms value for the secondary voltage in these cases is significantly higher. For increasing the boost-effect, the command tends to enlarge the duration of ST states during which the secondary  $LC$ -oscillator current is free to vary (see Fig. 14). The latter current is, therefore, more distorted (with total harmonic distortion touching 88.33% in the most severe case), and the assumptions of the proposed FHA-based approach are consequently less respected. A potential solution to this issue might be a supplemented control scheme with notably a higher switching frequency (which is though difficult

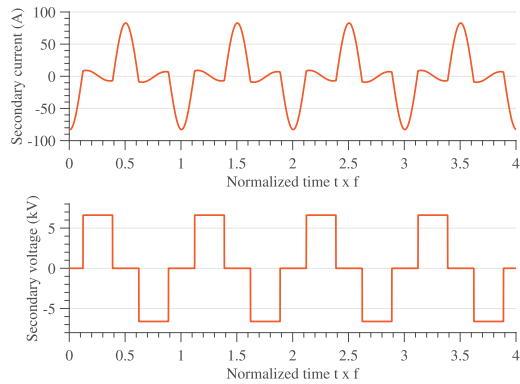


Fig. 14. Secondary current (up) and voltage (down) for a  $C_s$  deviation of  $-80\%$  impacting the improved system.

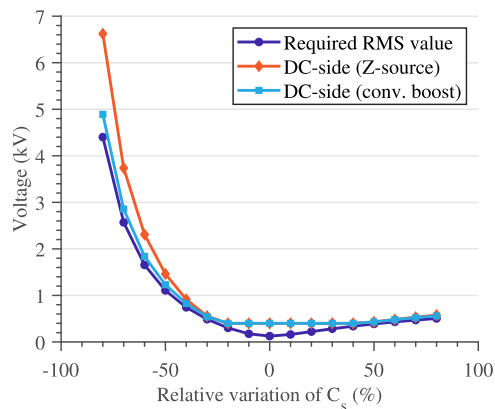


Fig. 15. Required dc voltage for ensuring a given voltage rms value (Z-source and conventional boost converters configurations).

to envision regarding the current state-of-the-art performances of switching devices in the targeted power range). Besides this operational concern, the Z-source converter presents an intrinsic practical issue, since it requires to raise the voltage rating for the circuit components. Indeed, from the ac-side of the converter, an increase of  $D_{ST}$  widens the zero-state in the ac voltage waveform, leading to a significant decrease of the rms value of the related fundamental as expressed mathematically by the sine argument in (28). For achieving a high voltage despite the rise of  $D_{ST}$ , the command scales up, therefore, the voltage  $V_h^A$  (which has to be supported by the switches). This is clearly observable in Fig. 15, where the rms voltage required by the proposed approach is contrasted with the related dc-side voltage using a Z-source converter. For comparison purposes, the related dc-side voltage using an additional conventional boost converter in cascade with the active rectifier is also represented.

## VI. CONCLUSION

In this article, a method employing an active rectification for the optimal control of a bidirectional resonant WPT system is proposed. Benefiting from a resonant dual active bridge topology, the real and, especially, the imaginary parts of the

equivalent load impedance can be modulated simultaneously and independently by controlling adequately the active rectifier switches. The command methodology development is based on a simple FHA (thanks to the important filtering effect provided by the resonant system) and ensures that the system delivers the required output power at its maximum achievable efficiency, despite sensible deviations in the circuit parameters. Using FHA, the effectiveness of the method has been shown and discussed against variations in the windings mutual inductance  $M$  (impacting the active power flow) and in the secondary capacitance  $C_s$  (impacting both the active and the reactive power flows). By extension, we acknowledged its effectiveness against any variation in any parameter in the circuit. The proposed converters topology and command have been implemented and simulated using a time-domain model, demonstrating the proposed method validity despite the noncompliance with the FHA assumptions (notably despite more realistic nonsinusoidal voltage waveforms).

Nevertheless, some controllability restrictions emerged with the time-domain implementation of the proposed methodology. Hence, the limitation in voltage producible by the converters reduces the compensation capabilities of the system, unable to produce a sufficient voltage for reaching the targeted optimal operating point in case of severe circuit parameters deviations. For surmounting these restrictions without requiring any additional converter, Z-source converters have been used. As exposed via a brief theoretical reminder, the Z-source topology allows the converters to produce any voltage between zero and infinity, notionally. The time-domain implementation of the improved topology (including Z-source instead of conventional converters) has demonstrated the removal of the aforementioned restrictions. Implemented on such a topology, the proposed method is capable to counter efficiently the most severe deviations in parameters as significant as the secondary resonator capacitance  $C_s$ . The establishment of a closed-loop control scheme and the constitution of a reduced power experimental prototype are envisioned as further work.

## REFERENCES

- [1] G. A. Covic and J. T. Boys, "Modern trends in inductive power transfer for transportation applications," *IEEE J. Emerg. Sel. Topics Power Electron.*, vol. 1, no. 1, pp. 28–41, Mar. 2013.
- [2] S. Li and C. C. Mi, "Wireless power transfer for electric vehicle applications," *IEEE J. Emerg. Sel. Topics Power Electron.*, vol. 3, no. 1, pp. 4–17, Mar. 2015.
- [3] K. A. Kalwar, M. Aamir, and S. Mekhilef, "Inductively coupled power transfer (ICPT) for electric vehicle charging—A review," *Renewable Sustain. Energy Rev.*, vol. 47, pp. 462–475, 2015.
- [4] R. Bosshard and J. W. Kolar, "Inductive power transfer for electric vehicle charging: Technical challenges and tradeoffs," *IEEE Power Electron. Mag.*, vol. 3, no. 3, pp. 22–30, Sep. 2016.
- [5] A. P. Sample, D. T. Meyer, and J. R. Smith, "Analysis, experimental results, and range adaptation of magnetically coupled resonators for wireless power transfer," *IEEE Trans. Ind. Electron.*, vol. 58, no. 2, pp. 544–554, Feb. 2011.
- [6] D. Patil, M. Sirico, L. Gu, and B. Fahimi, "Maximum efficiency tracking in wireless power transfer for battery charger: Phase shift and frequency control," in *Proc. IEEE Energy Convers. Congr. Expo.*, Sep. 2016, pp. 1–8.



- [7] C.-S. Wang, O. H. Stielau, and G. A. Covic, "Design considerations for a contactless electric vehicle battery charger," *IEEE Trans. Ind. Electron.*, vol. 52, no. 5, pp. 1308–1314, Oct. 2005.
- [8] H. Li, X. Yang, K. Wang, and X. Dong, "Study on efficiency maximization design principles for wireless power transfer system using magnetic resonant coupling," in *Proc. IEEE ECCE Asia Downunder*, Jun. 2013, pp. 888–892.
- [9] H. Li, J. Li, K. Wang, W. Chen, and X. Yang, "A maximum efficiency point tracking control scheme for wireless power transfer systems using magnetic resonant coupling," *IEEE Trans. Power Electron.*, vol. 30, no. 7, pp. 3998–4008, Jul. 2015.
- [10] W. X. Zhong and S. Y. R. Hui, "Maximum energy efficiency tracking for wireless power transfer systems," *IEEE Trans. Power Electron.*, vol. 30, no. 7, pp. 4025–4034, Jul. 2015.
- [11] K. Colak, E. Asa, M. Bojarski, D. Czarkowski, and O. C. Onar, "A novel phase-shift control of semibrigeless active rectifier for wireless power transfer," *IEEE Trans. Power Electron.*, vol. 30, no. 11, pp. 6288–6297, Nov. 2015.
- [12] C. Zhao, Z. Wang, J. Du, J. Wu, S. Zong, and X. He, "Active resonance wireless power transfer system using phase shift control strategy," in *Proc. IEEE Appl. Power Electron. Conf. Expo.*, Mar. 2014, pp. 1336–1341.
- [13] A. Berger, M. Agostinelli, S. Vesti, J. A. Oliver, J. A. Cobos, and M. Huemer, "A wireless charging system applying phase-shift and amplitude control to maximize efficiency and extractable power," *IEEE Trans. Power Electron.*, vol. 30, no. 11, pp. 6338–6348, Nov. 2015.
- [14] U. K. Madawala and D. J. Thrimawithana, "A bidirectional inductive power interface for electric vehicles in v2g systems," *IEEE Trans. Ind. Electron.*, vol. 58, no. 10, pp. 4789–4796, Oct. 2011.
- [15] A. Desmoort, O. Deblecker, and Z. De Grève, "Active rectification for the optimal control of bidirectional resonant wireless power transfer," in *Proc. Int. Symp. Power Electron., Elect. Drives, Autom. Motion*, Jun. 2018, pp. 756–761.
- [16] F. Z. Peng, "Z-source inverter," *IEEE Trans. Ind. Appl.*, vol. 39, no. 2, pp. 504–510, Mar.–Apr. 2003.
- [17] N. S. Gonzalez-Santini, H. Zeng, Y. Yu, and F. Z. Peng, "Z-source resonant converter with power factor correction for wireless power transfer applications," *IEEE Trans. Power Electron.*, vol. 31, no. 11, pp. 7691–7700, Nov. 2016.
- [18] W. Tianfeng, L. Xin, T. Houjun, D. Yayun, and Y. Xijun, "Modeling and advanced control of wireless power transfer system with z-source inverter," in *Proc. IEEE 2nd Annu. Southern Power Electron. Conf.*, Dec. 2016, pp. 1–6.
- [19] H. Zeng, X. Wang, and F. Z. Peng, "High power density z-source resonant wireless charger with line frequency sinusoidal charging," *IEEE Trans. Power Electron.*, vol. 33, no. 12, pp. 10148–10156, Dec. 2018.



**Alexis Desmoort** (Student Member, IEEE) received the master's degree in electrical engineering from the Faculty of Engineering, University of Mons, Mons, Belgium, in June 2015 and the Ph.D. degree with the Electrical Power Engineering Unit, Faculty of Engineering, University of Mons, in 2019.

His research works are focused on the resonant wireless power transfer computational electromagnetic modeling and to surrounding power converters control.

Mr. Alexis Desmoort received the Research & Development Award delivered by the SRBE/KBVE for his master's thesis on the former topic.



**Olivier Deblecker** (Member, IEEE) was born in 1971. He received the degree in civil electrical engineering from Faculty of Engineering of the University of Mons, Belgium, in 1995, and the Ph.D. degree in electrical engineering from Faculty of Engineering of the University of Mons, Belgium, in 2001, respectively.

He is currently a Lecturer and the Head of the Electrical Power Engineering Unit, Faculty of Engineering, University of Mons, Mons, Belgium. His main fields of interest include power electronics and

drives, computational electromagnetics (particularly at intermediate frequencies), microgrids, energy management systems, renewables integration, and optimization techniques.

Dr. Deblecker has been a member of the European Power Electronics and Drives Association since 2004.



**Zacharie De Grève** (Member, IEEE) received the Electrical and Electronics Engineering degree and the Ph.D. degree in electrical engineering from the Faculty of Engineering, University of Mons, Mons, Belgium, in 2007 and 2012, respectively.

He was a Research Fellow of the Belgian Fund for Research (F.R.S/FNRS) and is currently a Research and Teaching Assistant with the Electrical Power Department, University of Mons. His research effort is mainly dedicated to the development of machine learning approaches to support decision making in

modern electrical power networks with a high share of renewables and computational electromagnetics, particularly at intermediate frequencies.